Iranian (Iranica) Journal of Energy & Environment
Journal Homepage: www.ijee.net
IJEE an official peer review journal of Babol Noshirvani University of Technology, ISSN:2079-2115

Effect of Wind Load on Milad Tower and Adjacent Buildings Case study: Shed Adjacent to Tower

A. A. Sheikh Aleslami, H. Sadeghi*

Department of Civil Engineering, Damghan Branch, Islamic Azad University, Damghan, Iran

PAPER INFO

Paper history:
Received 07 January 2023
Accepted in revised form 14 March 2023

Keywords:
Computational fluid dynamics modeling
Milad tower
Shed
Wind load
Wind tunnel test

ABSTRACT

Tall buildings are subject to wind loads as one of the effective lateral loads. An analysis of the effect of wind on Milad Tower is presented in this research. The wind tunnel testing results and numerical modelling implemented in computational fluid dynamics (CFD) using ANSYS software. For the numerical simulation, the K-epsilon model has been used. The study evaluated the flow around the tower in several deformation states and compared it with a model where the tower is modeled rigidly in the wind tunnel. The maximum coefficient of negative pressure (suction) at the top of the tower structure equals to -1.95, which occurs at $\theta = 90^{o}$, and the maximum coefficient of the positive pressure equals +1. Since the buildings near the tower are located a short distance from the tower, the shed's structure, which is located near the tower, has also been investigated. With the aid of Tecplot software. The wind pressure coefficients obtained from the wind tunnel test were plotted. As part of the wind loading analysis in the single-span and two-span shed models, the model is rotated with a step of 5^{o} relative to the direction of wind application, and wind pressure is recorded.

doi: *10.5829/ijee.2023.14.03.10*

INTRODUCTION

A multifunctional tower located in Tehran, Iran, called Milad tower. With a height of 436 meters, the Milad Tower is the sixth tallest tower in the world and the fourth tallest telecommunications tower in the world. Considering that wind load is one of the effective lateral loads in the design of tall structures. It is vital to estimate the design loads accurately. The geometry of a building significantly influences the wind loads. It is imperative to use experimental tests (wind tunnels) or numerical modeling since design codes do not provide data on all geometries. For this study, wind tunnel testing and computational fluid dynamics (CFD) using ANSYS software was used to determine the effect of wind on the building.

Literature on wind action on structures is extensive; Blocken [1] provided a comprehensive overview. In addition, Baker [2] has outlined the past, present, and future of wind engineering. It was reported that Su et al. [3] used a wind tunnel experiment to examine the influence of wind loads on large open-pit coal sheds with porous gables. Using wind tunnel results from solid and open-gable coal sheds, they examined the effects of gable ventilation on overall aerodynamic loads, wind pressure distribution, and peak wind loads. From 2013 to 2016, Yang et al. [4] examined devastating wind-related disasters in East Asia, including those in Japan, Philippines, and China. Several post-disaster investigations are described in the report, including those conducted following the 2013 hurricane in Philippines. There was Hurricane Mujigae, two hurricane-related hurricanes in October 2015 in Guangdong, China, and a tornado in June 2016 in Yancheng, China. Considering the effects of lateral wind and earthquake loads on Milad Tower, Wilhelm et al. [5] evaluated the dynamic behavior of Milad Tower. A thorough study has been conducted to study the effects of wind on this tower by Yahyai et al. [6]. This study used several computational fluid dynamics methods to predict the wind loads on and

*Corresponding Author Email: hossein_sadeghi1984@yahoo.com
(H. Sadeghi)

Please cite this article as: A. A. Sheikh Aleslami, H. Sadeghi, 2023. Effect of Wind Load on Milad Tower and Adjacent Buildings Case study: Shed Adjacent to Tower, Iranian (Iranica) Journal of Energy and Environment, 14(3), pp. 289-300. Doi: 10.5829/ijee.2023.14.03.10

the wind currents around the wind turbines. These included extensive vortex simulations (LES), Reynolds mean Navier-Stokes equations (RANS), etc. In 2007, Katsumura et al. [7] investigated the effects of equivalent static wind load on a large-aperture cantilevered roof. Kim et al. [8] studied the characteristics of wind pressure on retractable dome roofs. The results of this study were based on wind tunnel experiments carried out on dome roofs of various height-to-span ratios (0.01-0.5). The peak pressure coefficients of closed dome roofs were compared with the current Japanese wind load code after examining the characteristics of the medium and peak pressure coefficients. Also, Sadeghi et al. [9] simulated hemispherical domes and investigated the influence of the flexibility coefficient on shape factor, comparing the results with those obtained in a wind tunnel. Using numerical modeling based on computational fluid dynamics, Sadeghi et al. [10] presented wind pressure coefficients on scalp domes. Uematsu et al. [11] examined spherical domes with different deflection-to-span and rise-to-span ratios for two turbulent boundary layers. In their study, Rajabi et al. [12] examined the wind effect on Y-shaped buildings and discussed the most critical loading scenarios. As a result of Cheng and Fu's [13] study, hemispherical domes have been investigated for turbulent and laminar boundary layer flow. A study by the authors found that the sensitivity of pressure distribution on the hemisphere decreased as the Reynolds number increased above (1-2) $\times 10^5$ for the turbulent boundary layer flow. Using machine learning techniques, Hu and Kwok [14] collected wind data for different cylindrical engineering structures at various Reynolds numbers and provided statistical aerodynamic estimations. Liu et al. [15] investigated how wind-induced rain (WDR) affected a retractable roof at the grand opening of a stadium and the structural responses induced by the rain. The flow structures of single-celled and double-celled tornadoes and their effects on the dome structure have been studied by Li et al. [16]. According to Sanyal and Dalui [17], numerical modeling is used to investigate how wind loads affect the Y-shaped building, and the changes in the dimensions of the plan determine how much wind force affects the structure. Verma et al. [18] investigated the pressure caused by wind on various low-rise structures using an experimental method. In this research and different states, single, double, triple, and quadruple domes that were placed parallel behind each other, were tested in the wind tunnel, and the pressure coefficients were calculated. Ayoubi et al. [19] present analytical modeling for the prediction of horizontal-axis wind turbines power generation in wind farms based on an analytical wake model.

This research involves the construction of a multi-spanning shed adjacent to the tower, as shown in Figure 1. Wind load's effect on the shed's structure was also examined.

Figure 2 shows the models examined in the wind tunnel, the wind tunnel, and the measurement device. It was conducted in a free-flow open circulation blow wind tunnel with an approximately 18 meters' length. The test

Figure 1. Tehran's Milad Tower and its surroundings

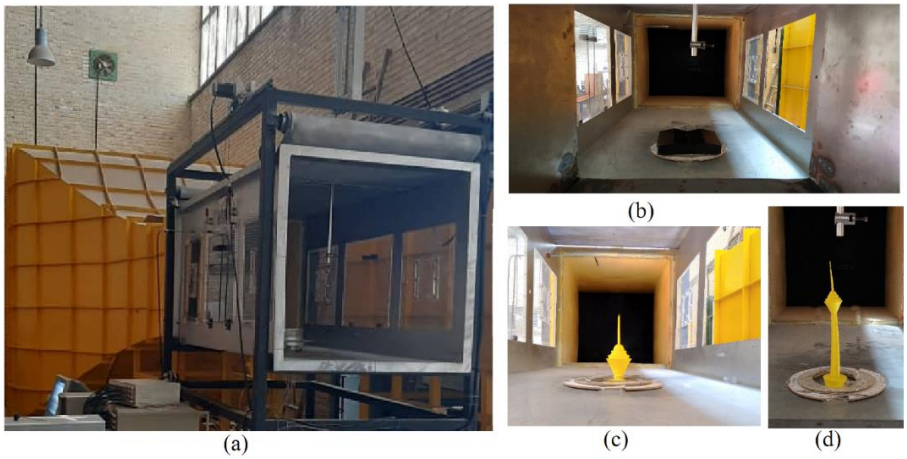

Figure 2. (a) Wind tunnel details, (b) shed model the wind tunnel, (c) Tower head structure model, and (d) Tower model in the wind tunnel

room had a width of 120 cm, a height of 120 cm, and a length of 300 cm. The unit had a centrifugal fan and a three-phase motor rated at 45 kW. Using a wind speed controller, the wind tunnel would produce a maximum wind speed of 35 m/s. The pressure measurement system consisted of a pressure transmitter, an analog-to-digital converter, a signal adaptor, a multimeter, a channel panel, a computer, and sensors with an outer diameter of 2 mm and an inner diameter of 1 mm. The wind speed was applied to the specimens to calculate the pressure coefficients at the pressure sensor locations. Sensors were placed at various angles with respect to the direction of the wind. Equation (1) shows the wind pressure coefficient is dimensionless.

$$C_P = \frac{\mathrm{P}}{0.5\rho \mathrm{V}^2} \quad (1)$$

here, ρ is the air density, P and V are the wind pressure and velocity, respectively.

Figure 3 illustrates the pressure measurement points on the Milad Tower head structure. To calculate the pressure coefficients in the tower perimeter, the structure is rotated five degrees in the wind tunnel each time, and the wind pressure is recorded. As a result, the amount of wind pressure at the tower's perimeter can be calculated and plotted in the figure. Under the geometric symmetry of the tower, the pressure is measured at an angle of 0 to 180 degrees for half of the structure. A model of a two-span shed structure with pressure measurement point is shown in Figure 4. During testing in the wind tunnel, the structure is rotated every five degrees and the wind pressure is measured to determine the most critical loading condition.

A contour plot of the wind pressure coefficients is drawn using the recorded pressure values for the shed's roof, as shown in Figure 5. As shown in Figure 6, the coefficients of wind pressure obtained from the wind tunnel test are plotted on the wall of the two-span shed structure. As seen in Figures 5 and 6, changes in wind pressure coefficients are evident due to changes in the angle at which the wind is applied to the structure.

Modeling procedure

This research was conducted using ANSYS software, a numerical modeling program based on the computational fluid dynamics method (CFD). Based on Reynolds-averaged Navier-Stokes (RANS) method, the k-epsilon model was used as a two-equation turbulence model (linear eddy viscosity models). Using two transport equations, the k-epsilon model solves the turbulent kinetic energy (K) and the eddy dissipation rate (epsilon). A classical k-epsilon model is commonly used to calculate eddy viscosity. It is derived from Boussinesq's linear eddy viscosity concept [20] and developed by Bardina et al. [21]. As the mean strain rate increases, Reynolds stresses change linearly. The Reynolds stresses in the eddy viscosity model are expressed as follows:

$$\tau_{tij} = 2\mu_t\left(S_{ij} - S_{nn}\delta_{ij}/3\right) - 2\rho k\delta_{ij}/3 \quad (2)$$

where μ_t is the eddy viscosity, S_{ij} is the velocity-averaged strain rate tensor, ρ denotes the viscosity, k represents the turbulent kinetic energy, and δ_{ij} is the Kronecker delta. As a function of the turbulent kinetic energy and turbulent dissipation rate, the eddy viscosity can be expressed as follows:

$$\mu_t = c_\mu f_\mu \rho k^2/\varepsilon \quad (3)$$

where c_μ is the model coefficient obtained by equilibrium analysis at high Reynolds numbers, while f_μ is the damping function. The damping function is defined based on the turbulent Reynolds number.

$$Re_t = \rho k^2/\varepsilon\mu$$
$$\text{as:} \quad f_\mu = \exp\left(-3.4/(1 + 0.02Re_t)^2\right) \quad (4)$$

Launder-Sharma's k-epsilon model turbulent transport equations are as follows:

I) Equation for turbulence energy transport:

$$\frac{\partial \rho k}{\partial t}+\frac{\partial}{\partial x_j}\left(\rho u_j \frac{\partial k}{\partial x_j}-\left(\mu+\frac{\mu_\tau}{\sigma_k}\right)\frac{\partial k}{\partial x_j}\right)=\tau_{tij}S_{ij}-\rho\varepsilon+\phi_k \quad (5)$$

II) Equation for turbulence dissipation transport:

$$\frac{\partial \rho \varepsilon}{\partial t}+\frac{\partial}{\partial x_j}\left(\rho u_j \varepsilon-\left(\mu+\frac{\mu_\tau}{\sigma_\varepsilon}\right)\frac{\partial \varepsilon}{\partial x_j}\right)=c_{\varepsilon 1}\frac{\varepsilon}{k}\tau_{tij}S_{ij}-c_{\varepsilon 2}f_2\rho\frac{\varepsilon^2}{k}+\phi_\varepsilon \quad (6)$$

$c_\mu = 0.09$, $c_{\varepsilon 1} = 1.45$, $c_{\varepsilon 2} = 1.92$ $\sigma_k = 1.0$, $\sigma_\varepsilon = 1.3$, $Pr_t = 0.9$

$$f_2 = 1-0.3\exp\left(-Re_t^2\right) \text{ and } Re_t=\frac{\rho k^2}{\mu\varepsilon} \quad (7)$$

$$\phi_k = 2\mu\left(\frac{\partial\sqrt{k}}{\partial y}\right)^2 \text{ and } \phi_\varepsilon = 2\mu\frac{\mu_t}{\rho}\left(\frac{\partial^2 u_s}{\partial y^2}\right)^2 \quad (8)$$

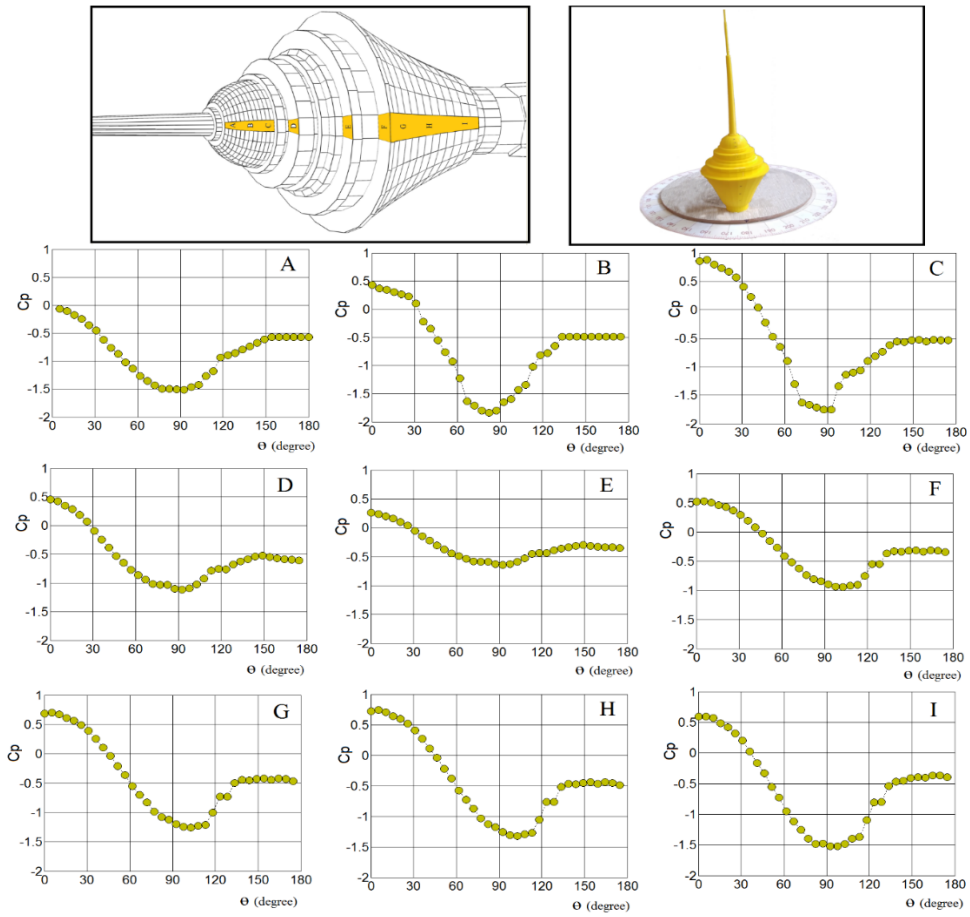

Figure 3. Wind pressure coefficients at different positions resulting from wind tunnel test

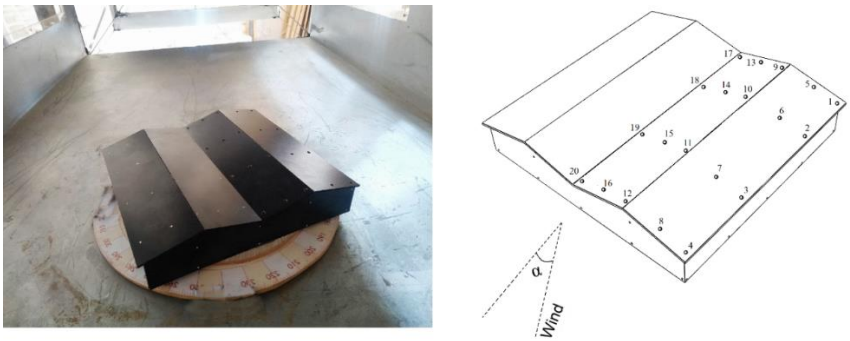

Figure 4. The pressure measurement points in the wind tunnel test on two-span shed structure

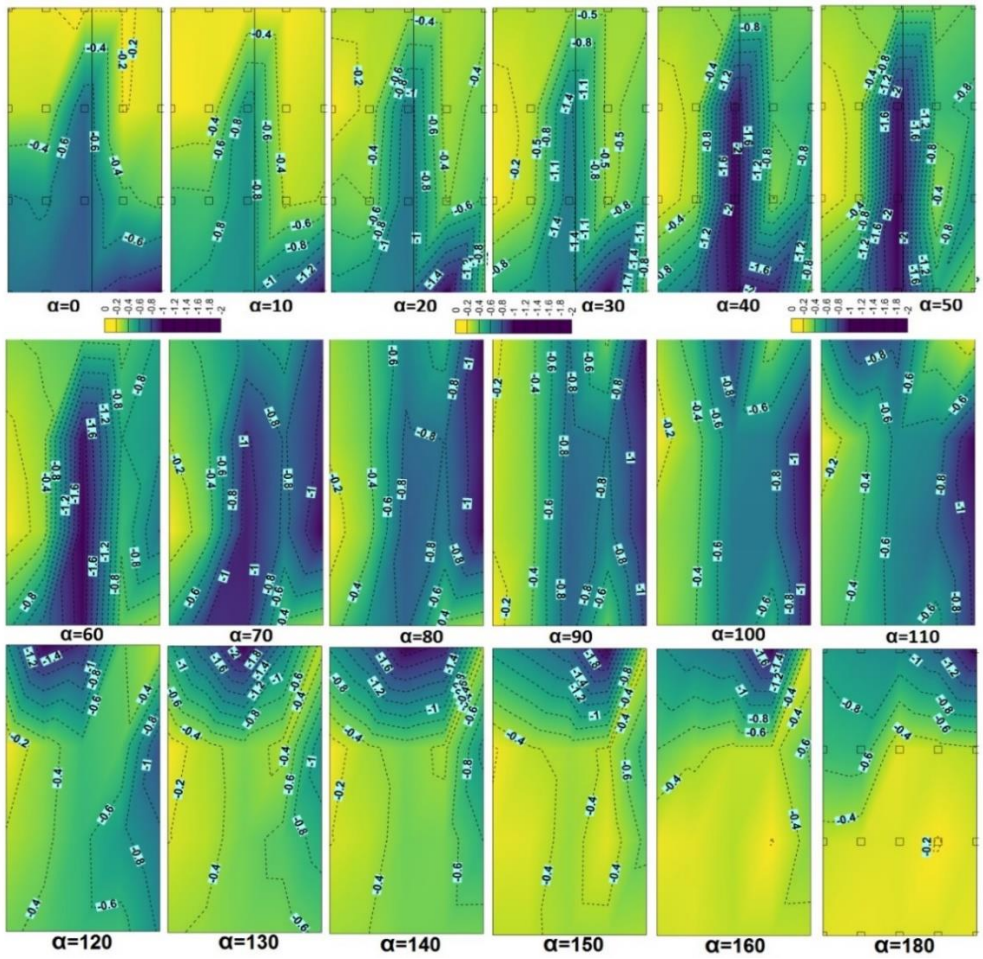

Figure 5. The Contour of wind pressure coefficients obtained from wind tunnel test on the roof of the shed

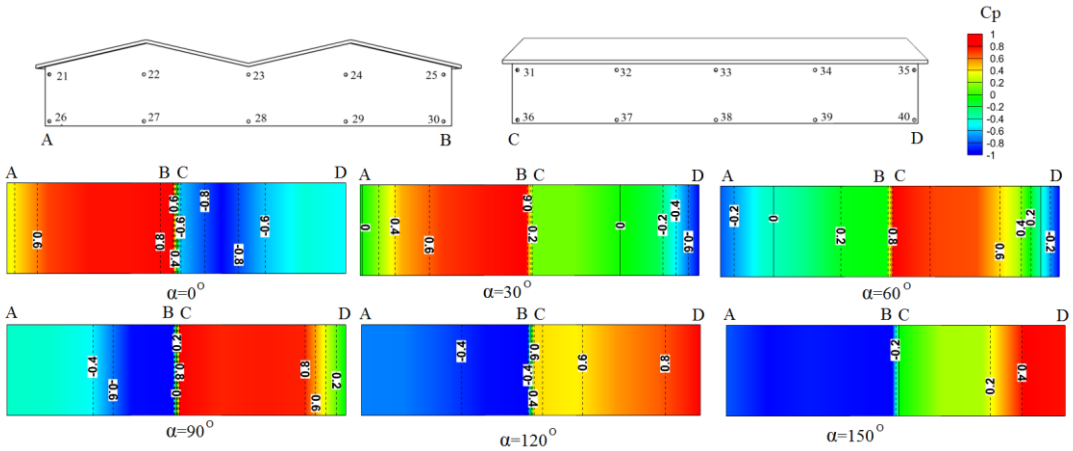

Figure 6. The contour of wind pressure coefficients obtained from wind tunnel test on the wall of the shed

Defining boundary conditions and analyzing grid sensitivity

Figure 7 illustrates the assumed boundary conditions in numerical modeling of wind tunnels along with wind tunnel dimensions and structural mesh models. As part of the numerical method, mesh, and sensitivity analysis is required, this means that the mesh dimensions must be assumed so that modeling results are not dependent on mesh dimensions. According to Figure 8, changing the mesh dimensions changes the pressure coefficients at the given points.

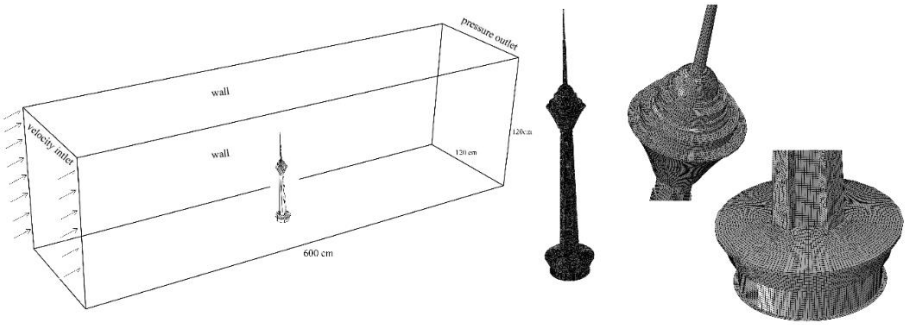

Figure 7. Boundary conditions of wind tunnel modeling in ANSYS software and mesh pattern on tower

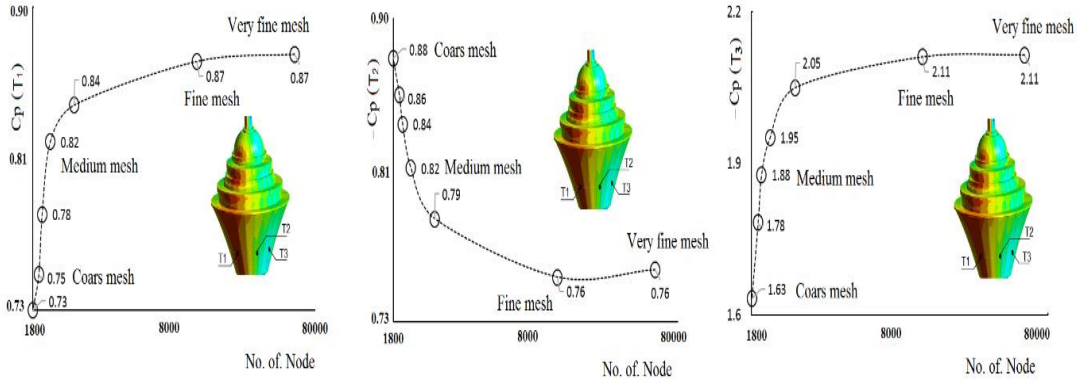

Figure 8. Mesh refinement test for Tower head structure

Figure 9 shows the lateral deformation of the tower as a result of wind load. A coupled ANSYS model has been used to obtain changes in wind pressure caused by the deformation of the structure. Defining the maximum displacement ratio to the tower height is the parameter ρ. In the case $\rho = 0$, a rigid structure is assumed. Streamlines around the tower are drawn to determine the effect of wind on the tower as a function of coefficient ρ. An illustration of the streamlines around a tower for different coefficients is shown in Figure 10. There is a correlation between a higher density of streamlines and a higher velocity. In some areas, vortices were observed. As a result of flow separation from the tower surface, these vortices were observed. Separation of flow indicates that wind flow has ceased to follow the tower shape and has instead separated from its surface, resulting in a reduction in lift. Even so, several variables influence flow separation, including the direction of the wind, its speed, and the shape of the surface. The wind pressure coefficient in vortex area became negative (a suction head). Figure 11 displays the changes of support reactions in z and y for varying coefficient ρ with respect to the state $\rho = 0$. Z and Y axes are defined concerning wind direction and vertical direction, respectively. The maximum support reaction of the support in the z-direction per ρ =0.008, which is 1.44 times the reaction of the support in the case where the tower is assumed to be rigid, and the maximum support reaction in the y-direction is obtained when the structure is assumed to be rigid.

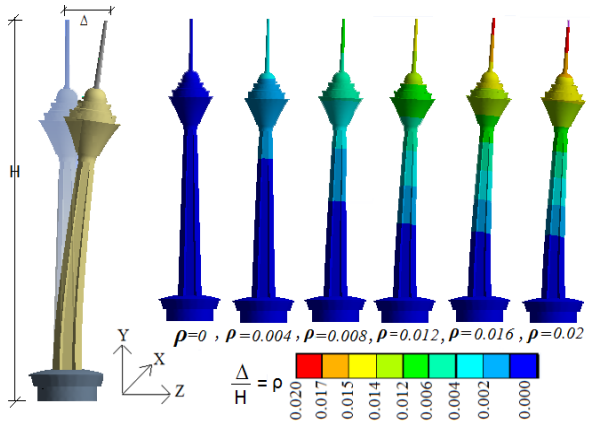

Figure 9. Contour deformation of the tower structure due to wind load

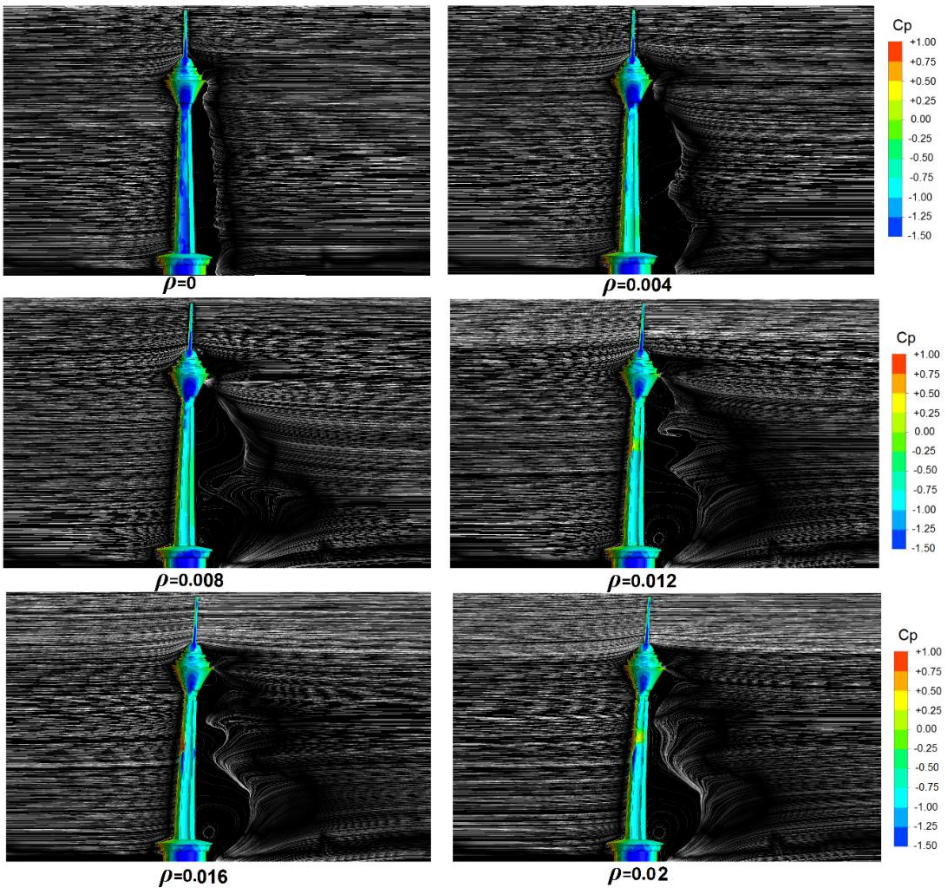

Figure 10. Streamlines around various models for different ρ coefficient

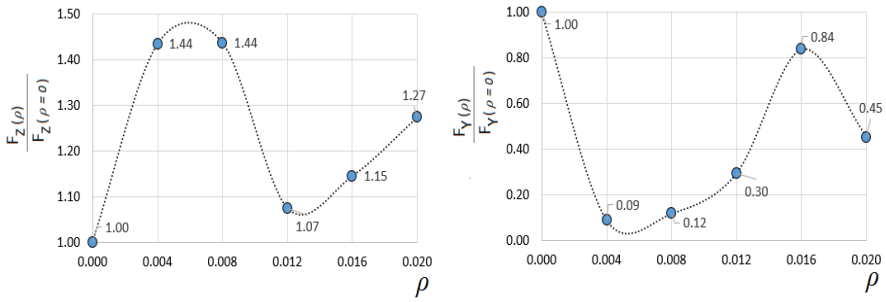

Figure 11. The direction of support reactions changes with respect to Z and Y according to the ρ coefficient

Interference effect

Considering the interaction of adjacent structures in determining the wind force of the design of the structures, the ' interference factor ', (dif) is defined in Equation (9). In this equation, parameters Cp_k and Cp_{0k} are wind pressure coefficient in the presence and absence of interference source(s), respectively (per measurement points, n).

$$(\text{dif}) = \sqrt{\frac{\sum_{k=1}^{n}(C_{pk}-C_{p0k})^2}{\sum_{k=1}^{n}(C_{p0k})^2}} \quad (9)$$

The effect of the Milad tower's proximity on the shed's structure has been investigated in two cases: the ratio of the tower's diameter to that of the shed is 0.5 and 3. By changing the distance between the two structures, the changes in support reactions in the shed structure are plotted in the direction of y and z. When $\frac{D}{D'} = 0.5$, the support reaction in the direction of Y and Z is approximately constant at intervals of 3.5 and 2.5, respectively. Also, where the ratio $\frac{D}{D'} = 3$, the support reaction in the direction of Y and Z is approximately constant at intervals of 1.5 and 1, respectively. Figure 12

shows the changes of parameter diff by changing the ratio of $\frac{S}{h}$ in the type: 2. The contour coefficients of wind pressure on the Milad Tower are shown in Figure 14. A positive pressure coefficient (pressure) is shown in the figure for the windward surfaces, and a negative pressure coefficient (suction) is indicated for the other surfaces.

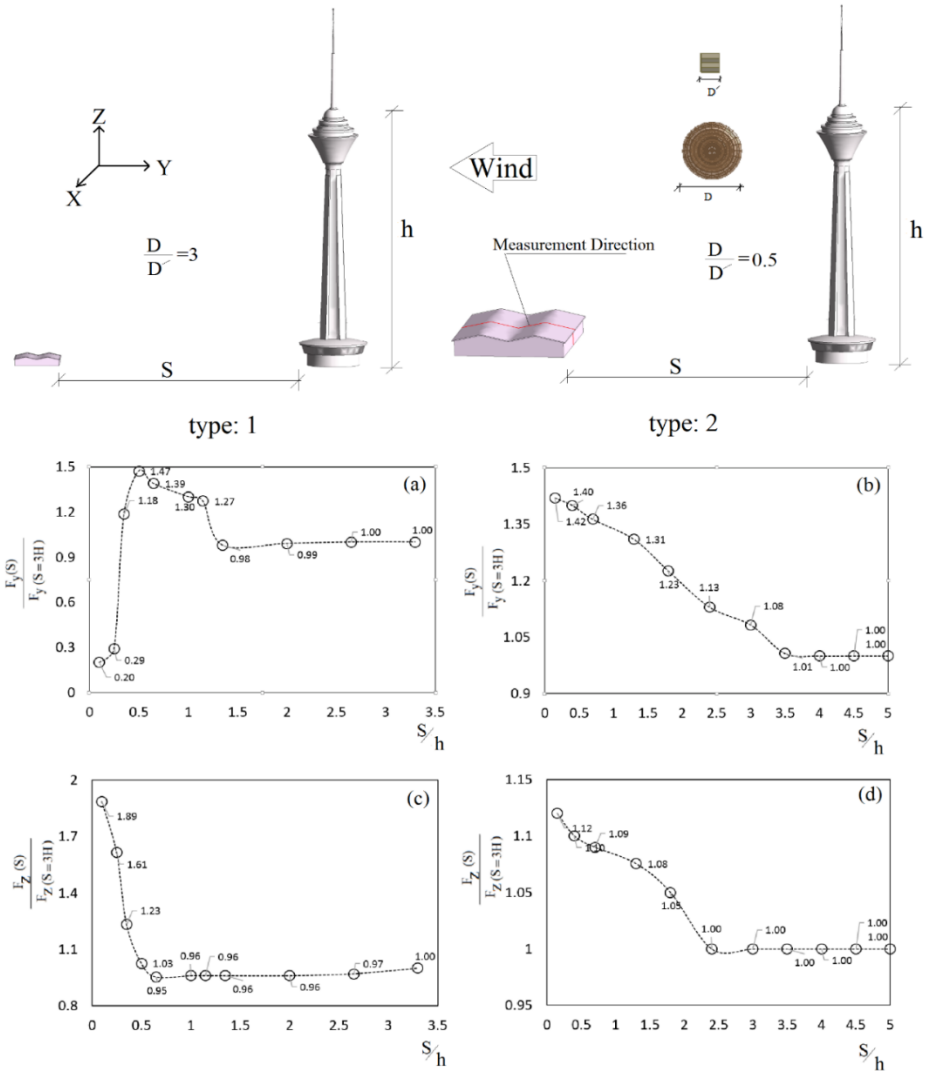

Figure 12. Support reactions change in the direction of Z and Y for different *S/h* ratio

Figure 15 plots wind pressure coefficients based on wind tunnel testing and numerical modeling. Figure 16 illustrates the wind pressure coefficients for a single-span shed structure. To find the most critical loading pattern for applying wind to the structure, it is changed in steps of 30 degrees from angle 0 to angle 150 °; in this figure, a diagram of the changes in the reaction of the support in the vertical direction is plotted for the changes in α, it is observed that the maximum value of the vertical reaction occurs at α = 60 and α = 120, and at the indicated angles the value of the image occurs. The action is 1.94 times with respect to α = 0.

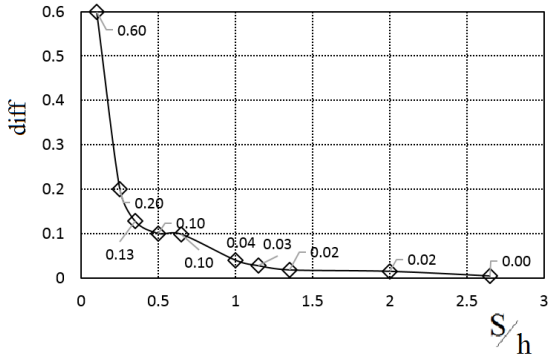

Figure 13. Changes to parameter diff by changing the ratio $\frac{S}{h}$

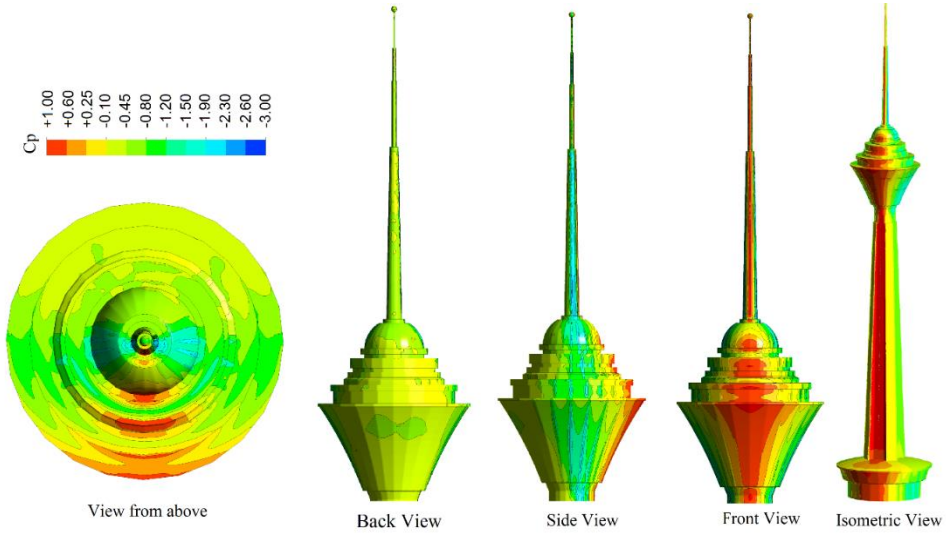

Figure 14. Distribution of wind pressure coefficients on the tower head structure

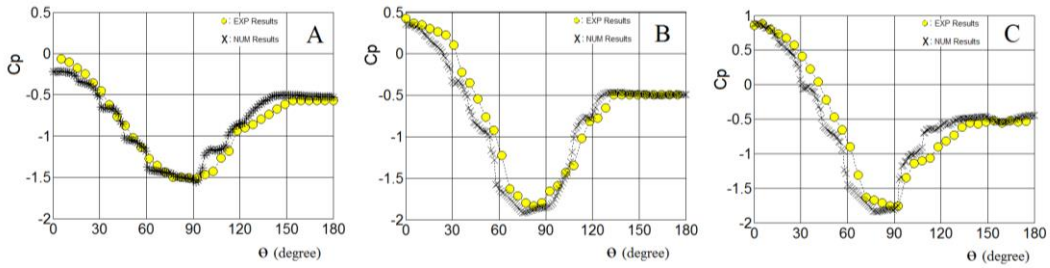

Figure 15. Comparison of pressure coefficients on the tower head structure for the k-ε model and experimental findings

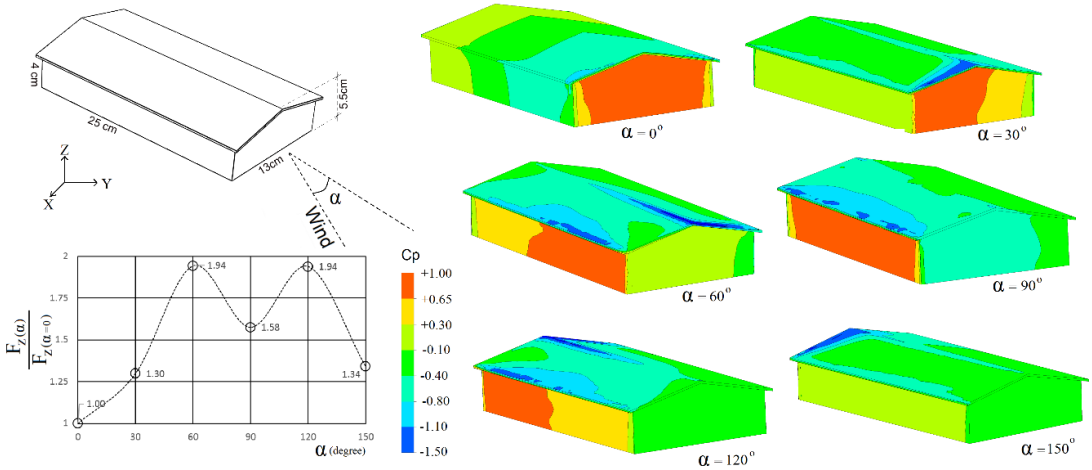

Figure 16. Distribution of wind pressure coefficients on the Single- span shed structure

Figure 17 illustrates the wind pressure coefficients for a two-span shed structure. To find the most critical loading pattern for applying wind to the structure, it is changed in steps of 30 degrees from angle 0 to angle 150°; in this figure, a diagram of the changes in the reaction of the support in the vertical direction is plotted for the changes in α, It is observed that the maximum value of the vertical reaction occurs at α = 0.

Figure 18 represents the wind pressure coefficients on the shed's wall with a two-span based on numerical modeling and wind tunnel tests.

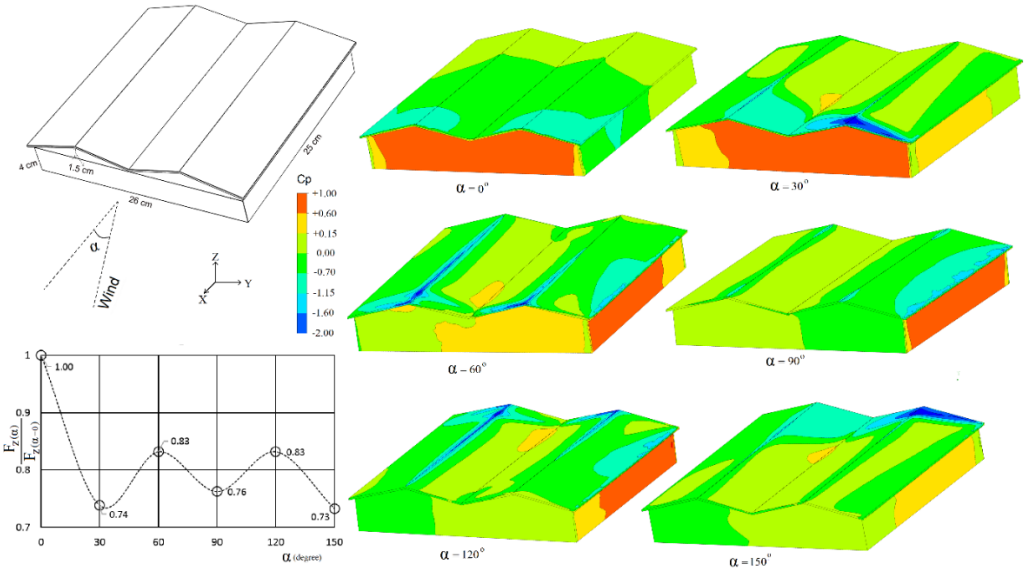

Figure 17. Distribution of wind pressure coefficients on the two-span shed structure

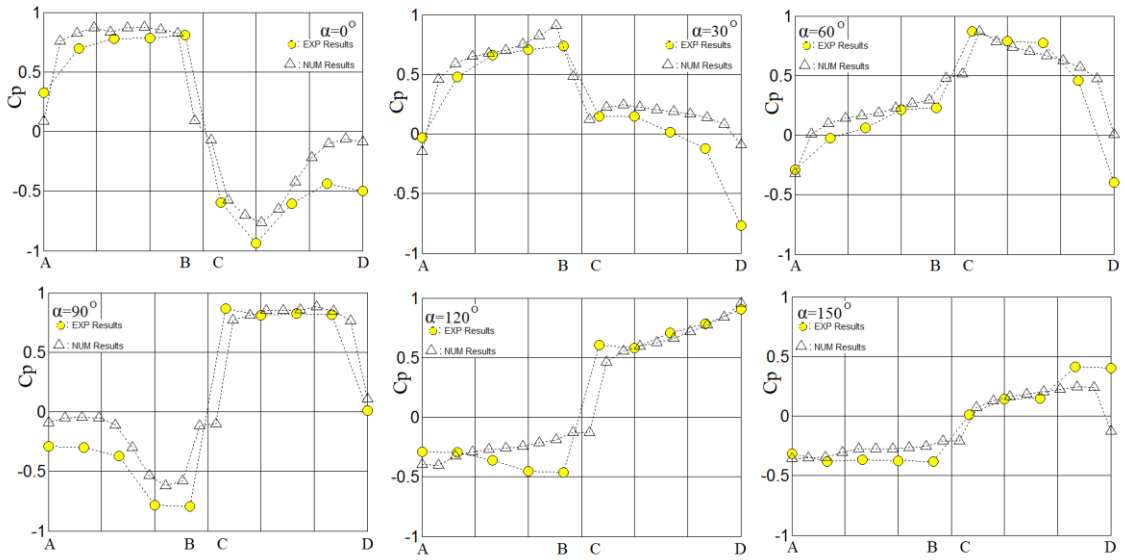

Figure 18. Comparison of pressure coefficients on the two-span shed structure for the k-ε model and experimental results

RESULTS AND DISCUSSION

The purpose of this paper was to describe the effect of wind load on the Milad tower. In addition, due to the presence of nearby structures, the effect of wind loads on the structure of single-span and double-span sheds was investigated using wind tunnel tests and numerical modeling**.**

1) According to Figure 3, the maximum coefficient of negative pressure (suction) at the top of the tower structure at point b is equal to -1.95, which occurs at the θ =90º. The maximum coefficient of positive pressure at point C is equal to +1. The θ =0º occurs, except for the surfaces facing the wind, where the pressure coefficients are positive; in most other cases, negative pressure coefficients are observed.

2) According to Figure 5, which shows the changes in the wind pressure coefficients resulting from the wind tunnel test for the roof of the shed, the maximum negative pressure (suction) equal to -2 is observed at α=50º; of course, for the design of the structure, all load case must be considered.

3) According to Figures 10 and 11, the effect of tower deflection on the changes of wind effect on the structure

can be seen, so that it can change the reaction of the support by up to 44%.

4) It is shown in Figure 12 how the Milad Tower relates to the wind force of its neighboring buildings in terms of effectiveness; if the distance of the neighboring buildings from the tower is equal to the height of the tower, it can be said that up to 90% of the effectiveness is lost. Both structures do not affect each other.

REFERENCES

1. Blocken, B., 2014. 50 years of Computational Wind Engineering: Past, present and future. *Journal of Wind Engineering and Industrial Aerodynamics*, 129, pp.69–102. Doi: 10.1016/j.jweia.2014.03.008
2. Baker, C.J., 2007. Wind engineering—Past, present and future. *Journal of Wind Engineering and Industrial Aerodynamics*, 95(9–11), pp.843–870. Doi: 10.1016/j.jweia.2007.01.011
3. Su, N., Peng, S., Hong, N., and Hu, T., 2020. Wind tunnel investigation on the wind load of large-span coal sheds with porous gables: Influence of gable ventilation. *Journal of Wind Engineering and Industrial Aerodynamics*, 204, pp.104242. Doi: 10.1016/j.jweia.2020.104242
4. Yang, Q., Gao, R., Bai, F., Li, T., and Tamura, Y., 2018. Damage to buildings and structures due to recent devastating wind hazards in East Asia. *Natural Hazards*, 92(3), pp.1321–1353. Doi: 10.1007/s11069-018-3253-8
5. Wilhelm, E., Ford, M., Coelho, D., Lawler, L., Ansourian, P., Alonso-Marroquin, F., and Tahmasebinia, F., 2016. Dynamic analysis of the Milad Tower. In: AIP Conference Proceedings. p 020006
6. Yahyai, M., Daryan, A.S., Ziaei, M., and Mirtaheri, S.M., 2011. Wind effect on milad tower using computational fluid dynamics. *The Structural Design of Tall and Special Buildings*, 20(2), pp.177–189. Doi: 10.1002/tal.522
7. Katsumura, A., Tamura, Y., and Nakamura, O., 2007. Universal wind load distribution simultaneously reproducing largest load effects in all subject members on large-span cantilevered roof. *Journal of Wind Engineering and Industrial Aerodynamics*, 95(9–11), pp.1145–1165. Doi: 10.1016/j.jweia.2007.01.020
8. YC, K., SW, Y., DJ, C., and JY, S., 2019. Characteristics of wind pressures on retractable dome roofs and external peak pressure coefficients for cladding design. *Journal of Wind Engineering and Industrial Aerodynamics*, 188, pp.294–307. Doi: 10.1016/j.jweia.2019.02.016
9. Sadeghi, H., Heristchian, M., Aziminejad, A., and Nooshin, H., 2018. CFD simulation of hemispherical domes: structural flexibility and interference factors. *Asian Journal of Civil Engineering*, 19(5), pp.535–551. Doi: 10.1007/s42107-018-0040-5
10. Sadeghi, H., Heristchian, M., Aziminejad, A., and Nooshin, H., 2017. Wind effect on grooved and scallop domes. *Engineering Structures*, 148, pp.436–450. Doi: 10.1016/j.engstruct.2017.07.003
11. Uematsu, Y., and Tsuruishi, R., 2008. Wind load evaluation system for the design of roof cladding of spherical domes. *Journal of Wind Engineering and Industrial Aerodynamics*, 96(10–11), pp.2054–2066. Doi: 10.1016/j.jweia.2008.02.051
12. Rajabi, E., Sadeghi, H., and Hashemi, M.R., 2022. Wind effect on building with Y-shaped plan. *Asian Journal of Civil Engineering*, 23(1), pp.141–151. Doi: 10.1007/s42107-022-00417-z
13. Cheng, C.M., and Fu, C.L., 2010. Characteristic of wind loads on a hemispherical dome in smooth flow and turbulent boundary layer flow. *Journal of Wind Engineering and Industrial Aerodynamics*, 98(6–7), pp.328–344. Doi: 10.1016/j.jweia.2009.12.002
14. Hu, G., and Kwok, K.C.S., 2020. Predicting wind pressures around circular cylinders using machine learning techniques. *Journal of Wind Engineering and Industrial Aerodynamics*, 198, pp.104099. Doi: 10.1016/j.jweia.2020.104099
15. Liu, M., Li, Q.S., and Huang, S.H., 2019. Large eddy simulation of wind-driven rain effects on a large span retractable roof stadium. *Journal of Wind Engineering and Industrial Aerodynamics*, 195, pp.104009. Doi: 10.1016/j.jweia.2019.104009
16. Li, T., Yan, G., Feng, R., and Mao, X., 2020. Investigation of the flow structure of single- and dual-celled tornadoes and their wind effects on a dome structure. *Engineering Structures*, 209, pp.109999. Doi: 10.1016/j.engstruct.2019.109999
17. Sanyal, P., and Dalui, S.K., 2021. Effects of side ratio for "Y" plan shaped tall building under wind load. *Building Simulation*, 14(4), pp.1221–1236. Doi: 10.1007/s12273-020-0731-1
18. Verma, A., Meena, R.K., Raj, R., and Ahuja, A.K., 2022. Experimental investigation of wind induced pressure on various type of low-rise structure. *Asian Journal of Civil Engineering*, 23(8), pp.1251–1265. Doi: 10.1007/s42107-022-00480-6
19. Ayoubi, P.A., Yazdi, M.E., and Harsini, I., 2022. Analytical Modeling for Prediction of Horizontal-Axis Wind Turbines Power Generation in Wind Farms Based on an Analytical Wake Model. *Iranian Journal of Energy and Environment*, 13(4), pp.398–407. Doi: 10.5829/IJEE.2022.13.04.09
20. Launder, B.E., and Sharma, B.I., 1974. Application of the energy-dissipation model of turbulence to the calculation of flow near a spinning disc. *Letters in Heat and Mass Transfer*, 1(2), pp.131–137. Doi: 10.1016/0094-4548(74)90150-7
21. Bardina, J.E., Huang, P.G., and Coakley, T.J., 1997. Turbulence modeling validation, testing, and development (No. A-976276).

Persian Abstract

چکیده

بار باد به عنوان یکی از بارهای جانبی موثر در ساختمان های بلند حائز اهمیت است. در این تحقیق تحلیلی از تأثیر باد بر برج میلاد با استفاده از نتایج آزمایش تونل باد و مدل‌سازی عددی با استفاده از دینامیک سیالات محاسباتی (CFD) با استفاده از نرم‌افزار ANSYS ارائه شده است. برای شبیه‌سازی عددی از مدل K-epsilon استفاده شده است. تغییرات جریان باد دراطراف برج در چندین حالت تغییر شکل سازه ارزیابی شده است و نتایج با حالتی که در آن برج به طور صلب در تونل باد مدل‌سازی گشته مقایسه شده است. حداکثر ضریب فشار منفی (مکش) در بالای سازه برج برابر با ۱.۹۵- است که در $\theta = 90^{o}$ رخ می‌دهد و حداکثر ضریب فشار مثبت برابر با ۱+ است. با توجه به اندرکنش سازه‌های مجاور تحت اثر بار باد، تاثیر برج میلاد بر سازه سوله‌ای که در نزدیکی برج قرار دارد نیز مورد بررسی قرار گرفته است. با کمک نرم افزار Tecplot ضرایب فشار باد به دست آمده از آزمایش تونل باد رسم می‌شود. به عنوان بخشی از تحلیل بارگذاری باد در مدل‌های سوله تک دهانه و دو دهانه، مدل با گام‌های ۵ درجه نسبت به جهت اعمال باد چرخانده شده و فشار باد ثبت شده است.